Kink boundaries and their role in dynamic recrystallisation of a Mg-Zn-Y alloy

Wu, Jing; Ikeda, Ken ichi; Shi, Q.; Chiu, Yu Lung

DOI:
10.1016/j.matchar.2018.12.027

Document Version
Peer reviewed version

Citation for published version (Harvard):
Wu, J, Ikeda, KI, Shi, Q & Chiu, YL 2019, 'Kink boundaries and their role in dynamic recrystallisation of a Mg-Zn-Y alloy', *Materials Characterization*, vol. 148, pp. 233-242. https://doi.org/10.1016/j.matchar.2018.12.027

Kink boundaries and their role in dynamic recrystallisation of a Mg-Zn-Y alloy

Jing Wu[1*], Ken-ichi Ikeda[2], Q. Shi[3,4], YuLung Chiu[1]

[1] School of Metallurgy and Materials, University of Birmingham, B15 2TT, UK

[2] Division of Materials Science and Engineering, Faculty of Engineering, Hokkaido University, 060-8628, Japan

[3] Department of Materials, Loughborough University, LE11 3TU, UK

[4] Guangdong Institute of Materials and Processing, Guangdong Academy of Sciences, 510650, China

[*] Email: J.Wu.6@bham.ac.uk

Abstract: An as-cast $Mg_{94}Zn_2Y_4$ alloy has been subjected to compression and equal channel angular pressing separately; the resultant microstructure was characterised using scanning electron microscopy (SEM), transmission electron microscopy (TEM) and transmission Kikuchi diffraction (TKD). The as-cast $Mg_{94}Zn_2Y_4$ alloy contains a long-period stacking ordered (LPSO) phase and a $Mg_{24}Y_5$ phase. After the compression, kink boundaries are observed in the LPSO phase and are composed of straight basal <a> dislocations. The dislocation arrangement in the kink boundaries of the LPSO/Mg mixture (alternate thin layers of LPSO and Mg) is similar to that in the LPSO phase. The rotation axes of the kink boundaries in LPSO/Mg are preferentially located in the (0001) plane, though [0001] rotation axis has occasionally been observed. Double kinking and non-basal slip have also been observed in the LPSO/Mg mixture. Dynamically recrystallised Mg grains are observed in the kink boundaries located within the LPSO/Mg mixture, preferentially in the kink boundaries with high misorientation angles. The kink boundary acts as the nucleation site for dynamic recrystallisation due to the high energy stored.

Kink boundaries and their role in dynamic recrystallisation of a Mg-Zn-Y alloy

Jing Wu[1*], Ken-ichi Ikeda[2], Q. Shi[3,4], YuLung Chiu[1]

[1] School of Metallurgy and Materials, University of Birmingham, B15 2TT, UK

[2] Division of Materials Science and Engineering, Faculty of Engineering, Hokkaido University, 060-8628, Japan

[3] Department of Materials, Loughborough University, LE11 3TU, UK

[4] Guangdong Institute of Materials and Processing, Guangdong Academy of Sciences, 510650, China

[*] Email: J.Wu.6@bham.ac.uk

Abstract: An as-cast $Mg_{94}Zn_2Y_4$ alloy has been subjected to compression and equal channel angular pressing separately; the resultant microstructure was characterised using scanning electron microscopy (SEM), transmission electron microscopy (TEM) and transmission Kikuchi diffraction (TKD). The as-cast $Mg_{94}Zn_2Y_4$ alloy contains a long-period stacking ordered (LPSO) phase and a $Mg_{24}Y_5$ phase. After the compression, kink boundaries are observed in the LPSO phase and are composed of straight basal <a> dislocations. The dislocation arrangement in the kink boundaries of the LPSO/Mg mixture (alternate thin layers of LPSO and Mg) is similar to that in the LPSO phase. The rotation axes of the kink boundaries in LPSO/Mg are preferentially located in the (0001) plane, though [0001] rotation axis has occasionally been observed. Double kinking and non-basal slip have also been observed in the LPSO/Mg mixture. Dynamically recrystallised Mg grains are

observed in the kink boundaries located within the LPSO/Mg mixture, preferentially in the kink boundaries with high misorientation angles. The kink boundary acts as the nucleation site for dynamic recrystallisation due to the high energy stored.

Keywords: LPSO phase; kink boundary; dislocation analysis; dynamic recrystallisation

1. Introduction

Mg alloys are highly desirable for structural weight-saving applications, especially for their use in the automotive and aerospace industries due to their low density. Kawamura et al. [1] reported that a $Mg_{97}Zn_1Y_2$ alloy prepared by rapid solidification and powder metallurgy (RS/PM) has a yield strength around 600 MPa and ductility of about 5%, resulting from its nano-scale grain size and the dispersed long period stacking ordered (LPSO) phase. The deformation mechanism of the LPSO phase has since become the focus of extensive studies [2-11].

Kinking [2, 12] is an important deformation mode of LPSO despite the dominant basal <a> slip [2, 3] and less common non-basal <a> slip [3-6]. The kink bands in the LPSO phase exhibit different crystal orientation relationships with respect to the matrix, i.e. without a fixed rotation axis and with different rotational angles [8]. Yamasaki et al. [9] divided the rotation axes into three types: $\langle 1\bar{1}00\rangle$ (here the LPSO structure is described as a hexagonal structure), $\langle 0001\rangle$ and $\langle 1\bar{2}10\rangle$ type rotation axes. Hagihara et al. [7, 8] further proposed that the rotation axis are mainly $\langle uvw0\rangle$ type in a wide range when LPSO sample was compressed with most grains parallel to $[1\bar{2}10]$ zone axis. Hagihara et al. [3] suggested the formation of kinks in LPSO phase can be explained by Hess and Barrett's dislocation model [13]: the kink band is composed of dislocation pairs on many parallel planes, spaced regularly only a small number of atomic distances apart [7,13,14].

Matsumoto et al. [11] studied the dislocation arrangement in the low angle kink boundaries and revealed that the kink boundaries are composed of basal <a> type edge dislocations, whereby one or more of the Burgers vectors depend on the kink boundary rotation axes.

However, for most LPSO strengthened Mg-RE-Zn-based alloys [15-17], the LPSO mainly appears as a thin slice in the alternate Mg matrix and forms a LPSO/Mg structure. This multi-layered LPSO/Mg structure deforms in a combined manner [12, 18] and influences the recrystallisation behaviour of Mg [19-24]. For example, the Mg matrix in the interior of the LPSO phase was reported to deform in a similar manner to the kinking of the surrounding LPSO [12, 18]. Shao et al. [18] suggested that the thin Mg deformed via ½[0001] prismatic dislocations when the surrounding LPSO has kinked. However, previous studies hardly observed any <c> dislocations in the Mg matrix. Kim et al. [12] suggested that the Mg matrix was deformed by basal <a> slip and pyramidal <c+a> slip and the elastic modulus mismatch between the Mg matrix and the LPSO phase promoted the activation of non-basal slips. Thus, it is essential to clarify the origin of the kink deformation of the Mg/LPSO structure in comparison to the LPSO phase and to understand the effect of the kink boundaries on the recrystallisation of Mg. In this work, a $Mg_{94}Zn_2Y_4$ alloy was deformed and its dislocation arrangement was analysed, allowing for particular focus on the kink boundaries within the LPSO phase and the LPSO/Mg structure.

2. Experiments

The alloy used in this study was prepared by induction melting under an argon environment using pure Mg, pure Zn and Mg-30Y wt. % master alloys. The chemical composition of the $Mg_{94}Zn_2Y_4$

specimen was measured using EDS as $Mg_{94.25\pm0.32}Zn_{1.48\pm0.11}Y_{4.27\pm0.23}$ in at.% (hereafter named $Mg_{94}Zn_2Y_4$).

Samples with dimensions of 6 mm × 6 mm × 12 mm were cut from the as-cast ingot using a CUT 20 High Precision Wirecut EDM machine and then compressed at room temperature on a Zwick 1484 twin screw driven universal test machine with 200 kN load cell, utilising Zwick TestXpert2 software. The initial strain rate of the compression was about 5×10^{-4} s^{-1}. The first sample was compressed until failure (at about 20% strain) and the others were compressed to strains of 2%, 5%, 10% and 15%. Before the compression test, one surface of the sample was polished and marked with 11 spots each separated by 1 mm along the straight line parallel to the compression direction. This was achieved by using an automated Struers DuraScan-50 micro-hardness testing machine with a load of 0.2 kg. SEM images were taken from the same regions of interest before and after the compression test.

Equal channel angular pressing (ECAP) was also carried out on the as-cast $Mg_{94}Zn_2Y_4$ alloy. Specimens of 10 mm (width) × 10 mm (height) × 20 mm (length) were cut out from the as-cast alloy using the EDM machine. The specimens were ECAP processed for 3 passes at 300 °C with back pressure. The channel angle Φ and the outer arc angle Ψ of the ECAP die were 90° and 36°, respectively. The specimen was rotated 90 degrees between two consecutive passes.

After the compression and ECAP, the microstructure of the samples was analysed on a JEOL 2100 transmission electron microscope (TEM). The TEM samples were prepared by twin-jet electropolishing using a solution containing 8.8 g lithium chloride, 19.3 g magnesium perchlorate, 833 mL methanol, and 167 mL butoxyethanol at -30 °C and 70 V. Transmission Kikuchi

Diffraction (TKD) was then used to obtain the crystal orientation information of the thin TEM sample.

3. Results and discussion

3.1 Kink boundary in the LPSO phase

Figure 1(a-b) presents the backscattered electron images obtained from the as-cast $Mg_{94}Zn_2Y_4$ alloy. A dense distribution of secondary phases forming a network can be observed in the Mg matrix. The Mg phase has a dendritic morphology with the secondary phases inside the dendritic arms. Two types of secondary phases can be distinguished based on the BSE images. The plate-shaped LPSO phase has the average chemical composition of $Mg_{87.48+0.33}Zn_{4.91+0.13}Y_{7.61\pm0.20}$ at.%. The brighter $Mg_{24}Y_5$ phase has the average composition of $Mg_{86.43\pm0.70}Zn_{0.83\pm0.23}Y_{12.74\pm0.78}$ at.%. Figure 1(c-d) shows that the LPSO layers inside a Mg grain have different thicknesses but have the same orientation relationship with the Mg matrix, i.e. $(0001)_{LPSO}//(0001)_{Mg}$, consistent with the fact that the LPSO layers are aligned in the same direction within one grain (Figure 1a). The microstructure containing thin LPSO lamellae with alternating Mg lamellae is named LPSO/Mg structure.

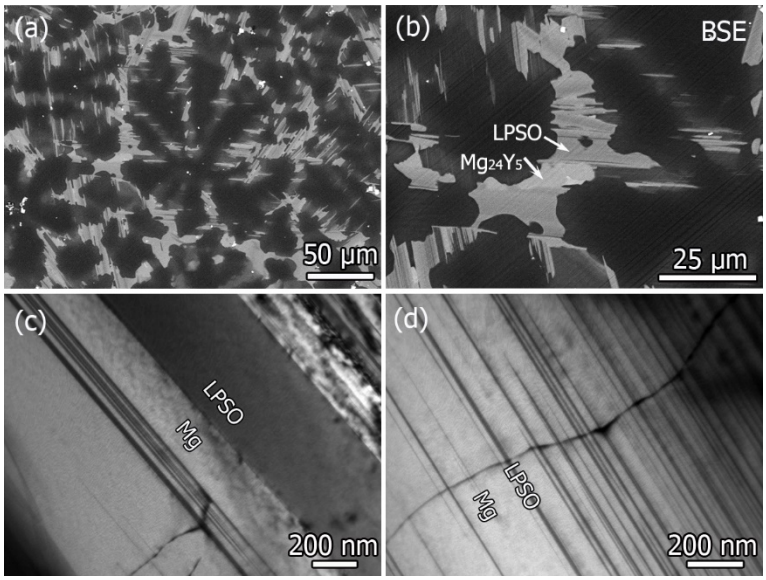

Figure 1(a) Backscattered electron images obtained from the as-cast $Mg_{94}Zn_2Y_4$ alloy showing prolific secondary phases; (b) higher magnification image showing two secondary phases; (c, d) TEM bright field images obtained from the as-cast $Mg_{94}Zn_2Y_4$ alloy showing the LPSO lamellae with different thicknesses.

The as-cast $Mg_{94}Zn_2Y_4$ samples were compressed to different strains, and the true strain-nominal stress curves are shown in Figure 2. The proof stress at 0.2% strain is about 185 MPa. Figure 3 shows SEM images obtained from the surfaces of the as-cast and the as-compressed samples. No obvious change can be observed in the sample with only 2% strain (Figure 3a versus Figure 3d) using SEM. More detailed TEM analysis of the 2% strain sample will be presented in Figure 4. When compressed to 10%, slip traces can be observed as indicated by yellow dashed lines in Figure 3e. After compressed to 20% strain, besides slip traces, there are obvious kink bands (indicated by the red arrows) observed in Figure 3f. The two kink bands show a beak-like shape and are almost perpendicular to the basal plane of the LPSO phase

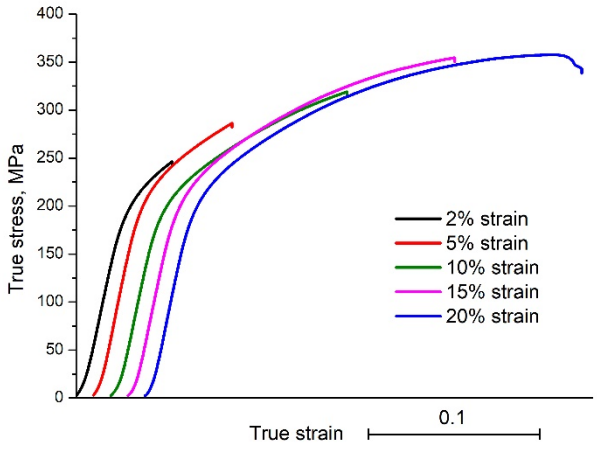

Figure 2 The true stress-strain curves obtained from the compression tests of the as-cast $Mg_{94}Zn_2Y_4$.

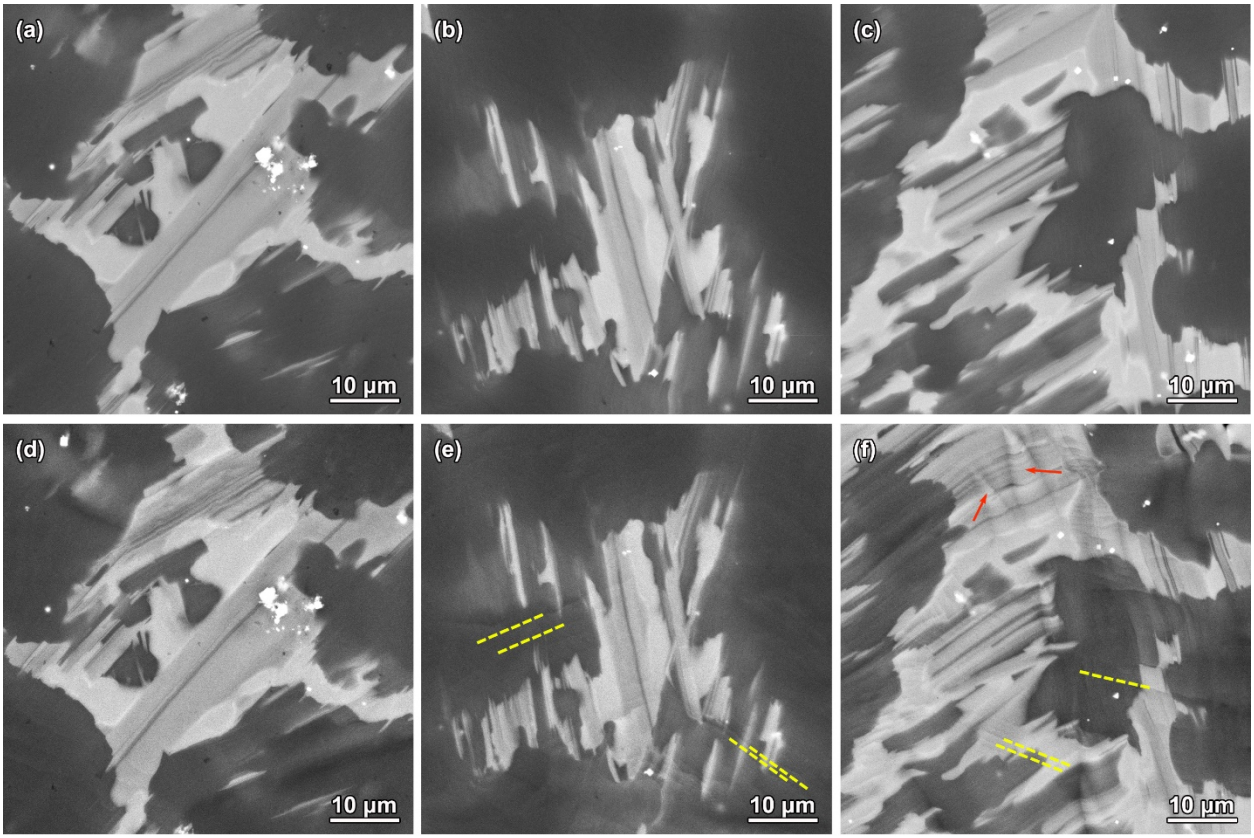

Figure 3 Comparision of LPSO phase before and after compression to different strains: (a-c) as cast samples before compression; (d-f) as-compressed samples corresponding to (a-c) with strains of 2%, 10% and 20%, respectively.

Figure 4a presents a bright-field TEM image obtained from the sample after 2% strain. A kink band (indicated by the yellow arrow) was found to cross through three separate LPSO lamellae. Similar to the twin boundary, the kink boundary separates the kinked material from the unkinked material. As shown in the higher magnification image in Figure 4b, the LPSO phase appears dark because the electron beam direction is close to the $[1\bar{2}10]$ zone axis. However, the kink band in the middle appears bright where the electron beam direction is clearly off the zone axis. The boundaries of the kink band (indicated as 4 and 5) are essentially dislocation walls, which are more obvious in Figure 4e. It is interesting to notice that there are other dislocation walls (labelled as 1, 2 and 3). They all lie in a direction almost perpendicular to the LPSO basal plane and are also kink boundaries. A closer view of dislocation walls 2 and 3 is shown in Figure 4c, where very straight basal dislocations can be observed. Different spacings between the dislocations within the walls indicate different misorientation angles. When imaged along $[1\bar{5}40]$ zone axis, the dislocations in kink boundary 5 are shown end-on, but the dislocations in kink boundary 4 still have a certain length (Figure 4d). This is particularly obvious when the dislocations are observed under the two-beam condition in Figure 4e, where the dislocation segments in kink boundary 5 now become very short and the dislocations in kink boundary 4 appear longer. It is interesting to notice that the dislocation spacing may vary within one kink boundary and that a large kink boundary may contain two or more small boundaries, e.g. kink boundary 5 consists of two smaller boundaries with larger dislocation spacings. Figure 4f shows the diffraction patterns taken from $[1\bar{5}40]$ confirming that the crystal rotates around the $[1\bar{5}40]$ zone axis; the misorientations caused by the kink boundary can be measured directly from the diffraction patterns.

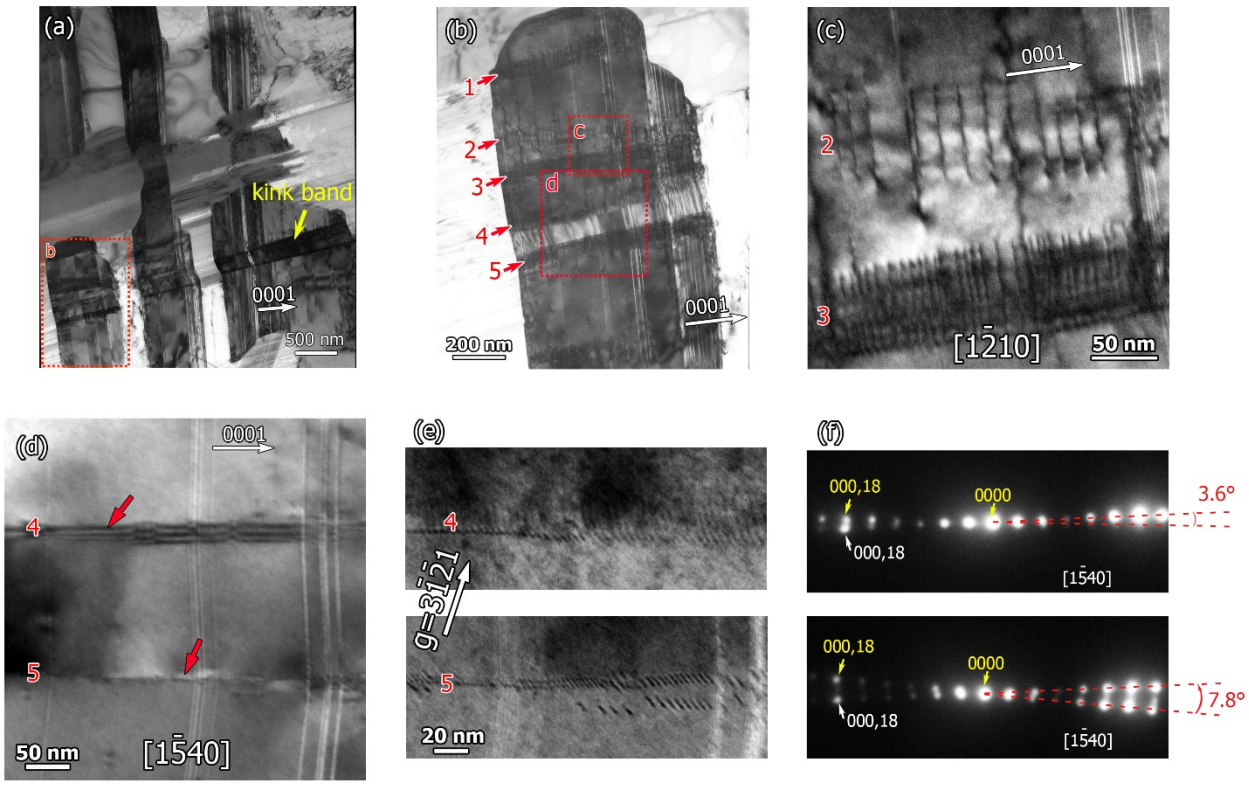

Figure 4 (a) TEM bright-field image obtained from the 2% compressed $Mg_{94}Zn_2Y_4$ alloy showing kink bands; (b) a magnified image from Region '*b*' in Figure 4a showing five dislocation walls in the LPSO phase. The electron beam direction is parallel to Mg [$1\bar{2}10$]; (c) a magnified image of LPSO phase from Region *c* showing the kink boundaries which contain straight and parallel dislocations on the basal plane. The electron beam direction is parallel to Mg [$1\bar{2}10$]; (d) a magnified image of Region *d* in Figure 4b observed along Mg [$1\bar{5}40$]; the dislocations in kink boundary 5 are end-on; (e) dislocation images taken under the two-beam condition with g = $3\bar{1}21$ and BD~ [$1\bar{5}40$] showing dislocation morphology. The top image corresponds to the kink boundary 4 region indicated by the top red arrow in Figure 4d whereas the bottom image corresponds to the region indicated by the red arrow in kink boundary 5; (f) SAD patterns taken from the kink boundaries regions in Figure 4d showing different misorientation angles. The top SAD pattern corresponds to kink boundary 4 and the bottom SAD pattern corresponds to kink boundary 5.

Figure 5a showing the lattice fringes of (0001) taken from kink boundary 5 suggests that the basal plane rotation caused by the kink boundary is about 7.6°, which is close to the 7.8° measured from

the diffraction pattern in Figure 4f. Figure 5b shows the dislocations in kink boundary 5 when the electron beam direction is close to the $[1\bar{2}10]$ zone axis. A closer look of the region using diffraction contrast indicates that there are two groups of dislocations as shown by the yellow arrows in Figure 5b.

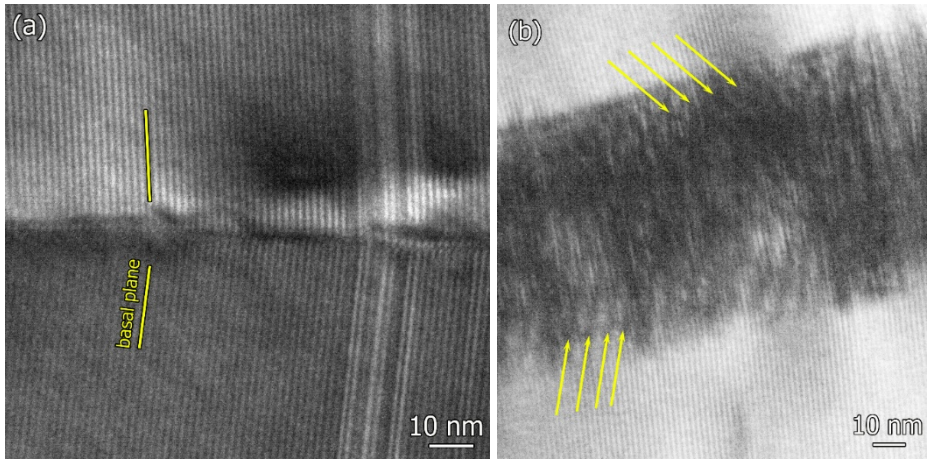

Figure 5 (a) High resolution TEM image of kink boundary 5 shows the basal plane rotating around the $[1\bar{5}40]$ zone axis; (b) Two groups of dislocations are found in the kink boundary, indicated by the different dislocation line directions. The electron beam direction is close to $[1\bar{2}10]$.

Figure 6a presents the dislocations in the LPSO phase in a 2% strain sample. Two groups of dislocations with distinct morphologies were observed. The dislocations in the kink boundary are straight and lie in the same direction, as indicated by the yellow arrow. The second group of dislocations (as indicated by the red arrow) are less straight and appear with different line directions. Different **g** vectors were used to identify their Burgers vectors. Figure 6a and 6c indicate all the dislocations were visible with $\mathrm{g} = \bar{1}10\bar{1}$ and $\mathrm{g} = 2\bar{1}\bar{1}0$, but they became out of contrast when imaged using $0\bar{1}12$ and 0002 reflections. This indicates the Burgers vectors of both groups

of dislocations are $\frac{1}{3}[2\bar{1}\bar{1}0]$, which is <a> type. When the beam direction is close to $[0\bar{1}10]$ (Figure 6(c)), it is noticed all the dislocations appear parallel to the basal plane, which indicates basal plane is the slip plane. Figure 6(d) shows on the right-side of the kink boundary (a dashed line is used to guide the eye), a hard phase ($Mg_{24}Y_5$) is found. This indicates the kink boundary is preferentially formed at a local stress concentration.

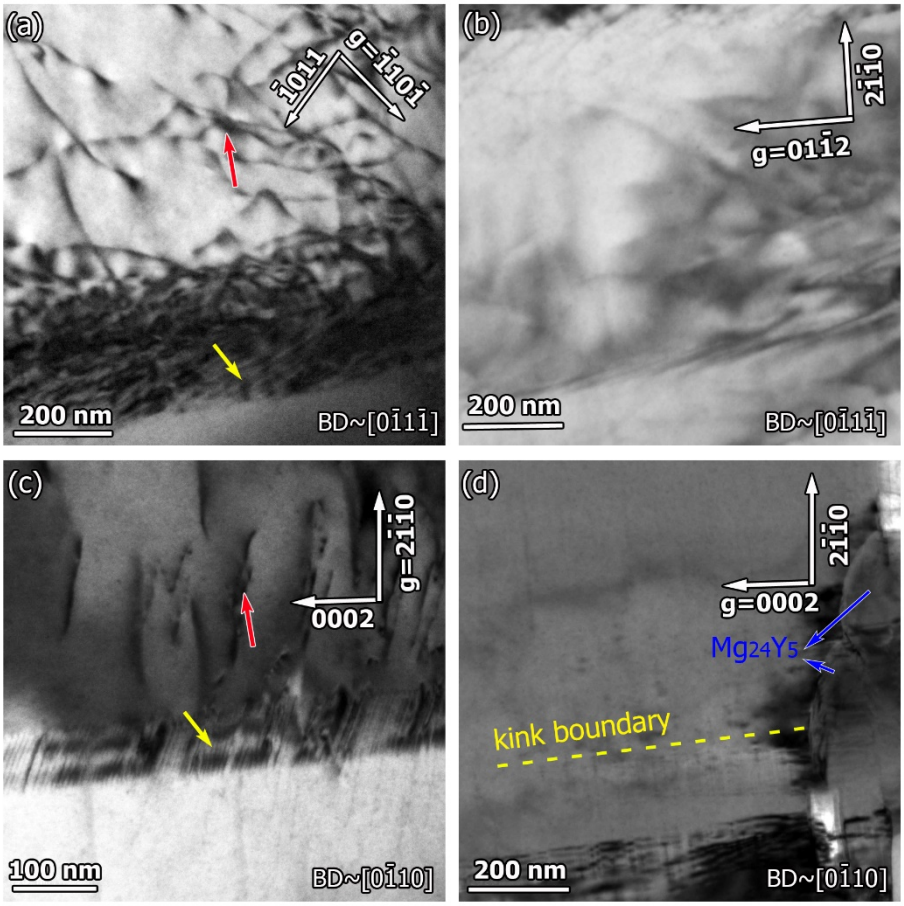

Figure 6 Dislocations in a kink boundary viewed under two-beam conditions using different reflection **g** vectors.

The kink boundaries with low misorientation angles are essentially low angle grain boundaries consisting of <a> type basal dislocations. The misorientation angles of the kink boundaries in Figure 4 can be measured directly by the rotation of the diffraction patterns or of the basal planes

themselves (Figure 5a). The edge dislocation spacing D in a low angle boundary can be linked to the misorientation angle shown in Equation 1,

$$D = \frac{b}{2\sin\theta/2} \qquad \text{Equation 1}$$

where **b** is the magnitude of the Burgers vector (0.3211 nm) and θ is the misorientation angle [25].

Table 1 shows the misorientation angles of the kink boundaries 1-5 displayed in Figure 4b and they have been measured directly from the rotation of the diffraction patterns and the basal planes. In addition, the misorientation angles resulting from the low angle grain boundaries have been calculated using the dislocation spacing D in Equation 1, assuming that they are simple tilt grain boundaries formed by pure edge dislocations. The average dislocation spacing D was measured directly from the TEM images. The calculated angles are in good agreement with the measured angles.

Table 1 Misorientation angles of kink boundaries in Figure 4b

Kink boundary	1	2	3	4	5
Directly measured angle, °	-	0.79	1.57	3.6	7.8
Average dislocation spacing D, nm	*14.7*	*14.4*	*7.39*	*4.18*	*2.1**
Angles calculated from dislocation spacing, °	1.30	1.28	2.32	3.592	7.1

*The average dislocation spacing of kink boundary 5 was measured using dislocations in the left part of the kink boundary 5 (see Figure 4); Figure 4e shows that kink boundary 5 contains one dislocation wall in the left part, whereas in the right part, it has been divided into two dislocation walls. In addition, the average dislocation spacings of the two small dislocation walls on the right are about 3.74 nm and 4.79 nm and the misorientation angles are calculated as 3.16 ° and 4.01 ° respectively. The sum of the two small kink boundaries is thus about 7.2 °.

The above results show that the low angle kink boundary in the LPSO phase is composed of geometrically necessary basal dislocations. In particular, a low angle kink boundary with $[1\bar{5}40]$ rotation axis has shown that the constituent basal dislocations have two line directions. According to Hess and Barrett's [13], when only one type of <a> dislocations exist, the rotation axis of the kink boundary is along $\langle 1\bar{1}00\rangle$. $[1\bar{5}40]$ is found between the $[1\bar{1}00]$ and $[0\bar{1}10]$ zone axes, which are probably composed of $\frac{1}{3}[11\bar{2}0]$ and $\frac{1}{3}[2\bar{1}\bar{1}0]$ dislocations by considering that the kink boundary is formed of geometrically necessary dislocations (GNDs) [11]. As a result of the different types of kinking that can be generated in the LPSO phase, it can accommodate the strains in various deformation directions. The typical kinking with $\langle 1\bar{1}00\rangle$ rotation axis can cause the titling of the basal plane, which leads to the movement of material along the c direction. Also, the kinking angle can be very high, e.g. 130º observed in [18], which suggests that large amounts of strain can be accomodated by kinking.

Figure 7 shows different dislocation configurations in the LPSO phase and the Mg matrix for the 2% strained sample. A small step is observed on the kind band in Figure 7a, as indicated by the yellow dashed lines which correspond to the kind boundaries. Figure 7b shows that within a kink band, discrete dislocations are observed. Compared to the dislocations in the kink boundaries, of which possess similar dislocation line directions and a very ordered arrangement, these dislocations within the kink band have morphologies. Figure 7c highlights the interaction between dislocations in the kink boundary and those on the outside of the kink boundary. Some dislocations (in the yellow dashed box) piled up ahead of a kink boundary (indicated by red arrow) and formed arrays perpendicular to the kink boundary. This suggests that the dislocation movement was hindered by the kink boundaries.

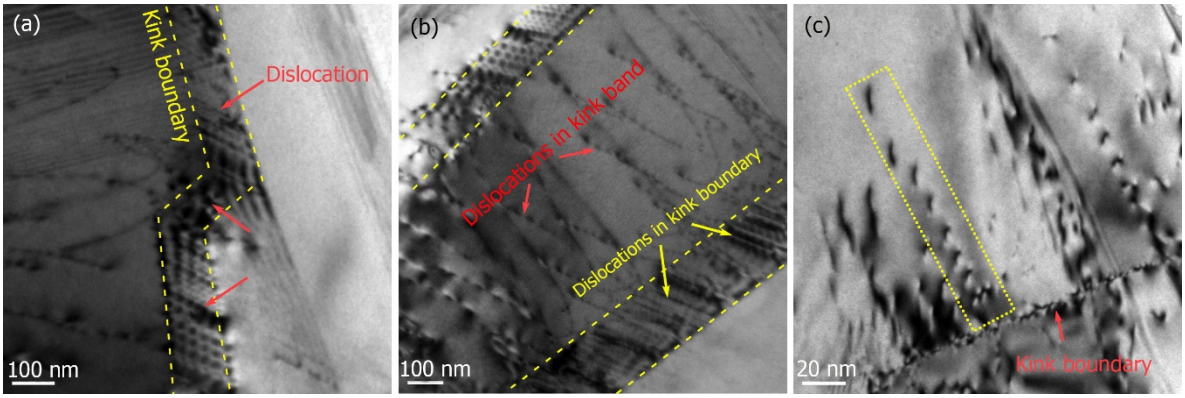

Figure 7 (a) TEM bright field image showing a kink boundary with a small step; (b) discrete dislocations in the kink band; (c) dislocations piled up on the kink boundary.

3.2 The kink deformation of LPSO/Mg in an ECAPed alloy

Figure 8a shows a TKD orientation map of the LPSO/Mg structure obtained from a 3-pass ECAPed sample where the corresponding forward scattered image is shown in Figure 8b. The Y map in Figure 8c confirms the thin bright phase as LPSO, which contains more Y than that in the Mg matrix and less Y than that in the $Mg_{24}Y_5$ particles in the lower-right corner. The LPSO phase lamella are very thin and their Kikuchi pattern is similar to Mg, so the orientation map only shows Mg. The deformed Mg phase contains sharp boundaries and a zigzag shape, which is similar to the kinking in the LPSO phase. Some kink boundaries ended inside the Mg alloy (black arrow) and some high angle kink boundaries transformed into several low angle kink boundaries (white arrow). The rotational axes of the kink boundaries are shown in Figure 8d where the maxima of the contour map can be found at $[\bar{1}2\bar{1}0]$. This indicates that the kink boundaries are mainly rotated along the $[\bar{1}2\bar{1}0]$ zone axis. A relatively high density of rotational axes is distributed in a ring connecting the $[\bar{1}2\bar{1}0]$ and $[01\bar{1}0]$ zone axes. The rotational axes observed can be regarded as a combination of $\langle 1\bar{1}00\rangle$ and $\langle 0\bar{1}10\rangle$ as proposed in [76].

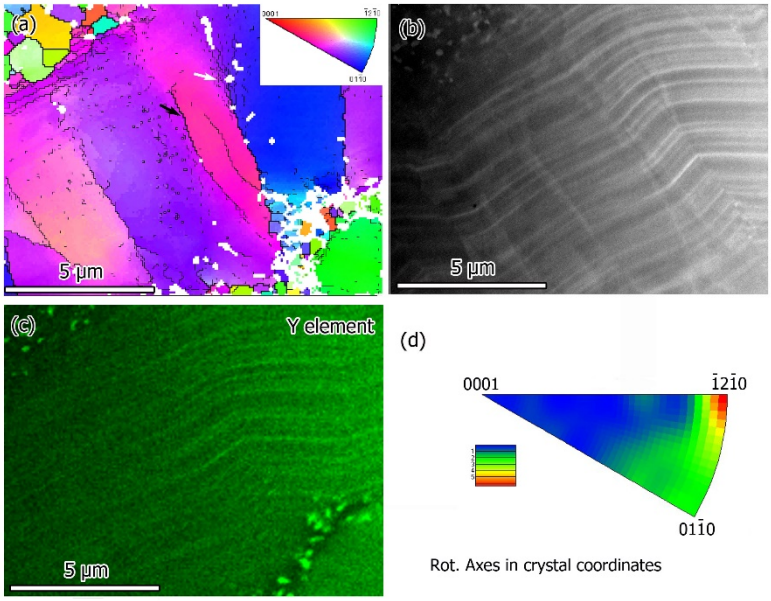

Figure 8 (a) Orientation map of Mg phase in the 3-pass ECAPed sample. Low angle boundaries (2°~10°) are indicated by thin black lines, high angle boundaries (>10°) by thick black lines, (b) forward scattered image; (c) EDS Y mapping; (d) rotational axis of the kink boundaries in crystal coordinates.

Figure 9a shows a TEM bright field image obtained from the LPSO/Mg structure in a 3-pass ECAP processed sample. It shows a clear kink boundary in the right-hand part of the image with a misorientation angle of about 68º, which has been measured directly from the basal planes. The low angle kink boundaries, on the other hand, are less obvious in the TEM image, indicated by the arrow in Figure 9a. Figure 9b shows that the low angle kink boundary (corresponding to the arrowed area) contains numerous dislocations. In order to understand the crystallographic nature of the kink boundaries, the same area was characterised by TKD. The orientation map is shown in Figure 9c, where low angle boundaries (with misorientation angles of 2~10°) are indicated by thin black lines and high angle boundaries (with misorientation angle >10°) are indicated by thick black lines. It is interesting to notice that kink boundaries I and II are almost parallel to each other, and

have similar misorientation angles of about 16°. The areas outside of kink boundaries I and II have similar orientations. The rotational zone axis contour maps of kink boundaries I and II (Figure 9d) show that their maxima were both found to be close to the $[04\bar{4}1]$ zone axis. Therefore, the kink boundaries I and II belong to the same type, but with opposite rotation directions. A similar morphology was found in boundaries III and IV, which have smaller misorientation angles of about 4° and a rotation zone axis of [0001]. It is worth mentioning that kink boundaries III and IV are located inside kink boundaries I and II to form a morphology which is similar to double twinning. This phenomenon has not been reported elsewhere for the LPSO phase.

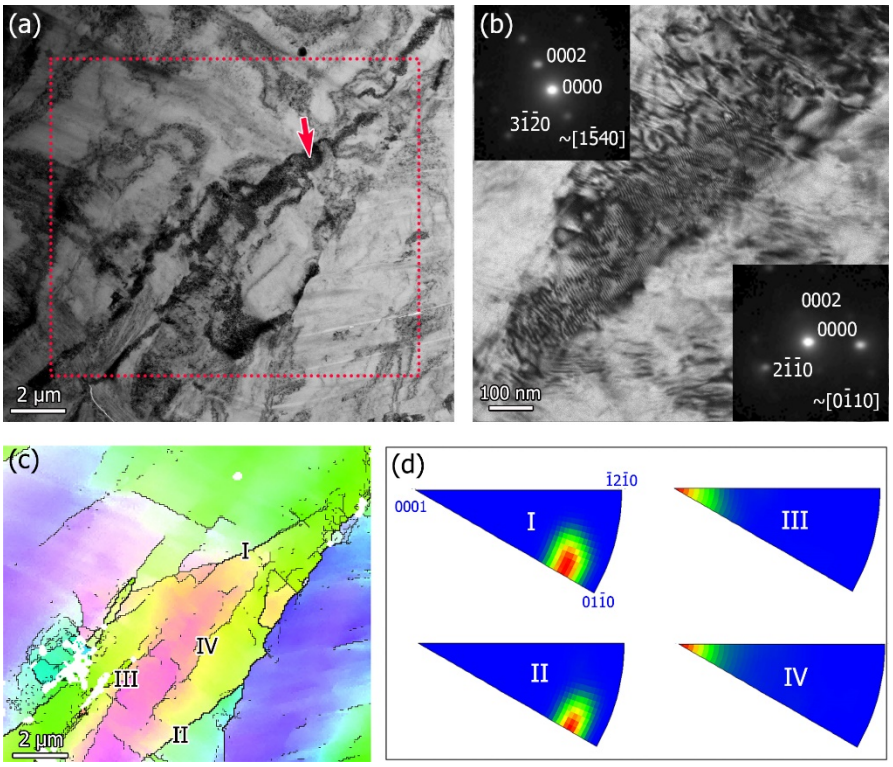

Figure 9 (a) TEM bright field image of the LPSO/Mg; (b) higher magnification image corresponding to the arrowed area in Figure 9a. The diffraction patterns were indexed as the closest zone axis (about 5° deviation); (c) orientation map showing paired kink boundaries in Mg/LPSO; (d) rotation axes of kink boundaries.

Figure 10a shows some of the kink boundaries dividing the LPSO/Mg structure into small domains. LPSO lamellae are shown as thin black lines in the Mg (indicated by the red dashed lines). The kink boundaries (indicated by yellow arrow in Figure 10a) show a rotational morphology, which has been described in [26]. The LPSO lamella shows a circular shape instead of a zigzag shape and allows for a continuous strain accommodated by the kink boundaries. In general, a large rotational angle can be obtained through series of low angle kink boundaries in the LPSO/Mg structure. Figure 10b shows a bright field image of a kink boundary in a LPSO/Mg structure. The misorientation angle of about 14.4° between the original and kinked areas was measured based on the basal plane orientation. Figure 10c shows another kink boundary in the LPSO/Mg region. The kink boundary contains a straight part, whose magnified image is presented in Figure 10d and indicates regularly arranged dislocations. Besides the straight kink boundary, a less straight section of the boundary is also indicated by blue arrows in Figure 10c. This is probably because there are different types of dislocations forming the kink boundary. Alternatively, different dislocation arrangements in the kink boundary may also lead to a wavy kink boundary.

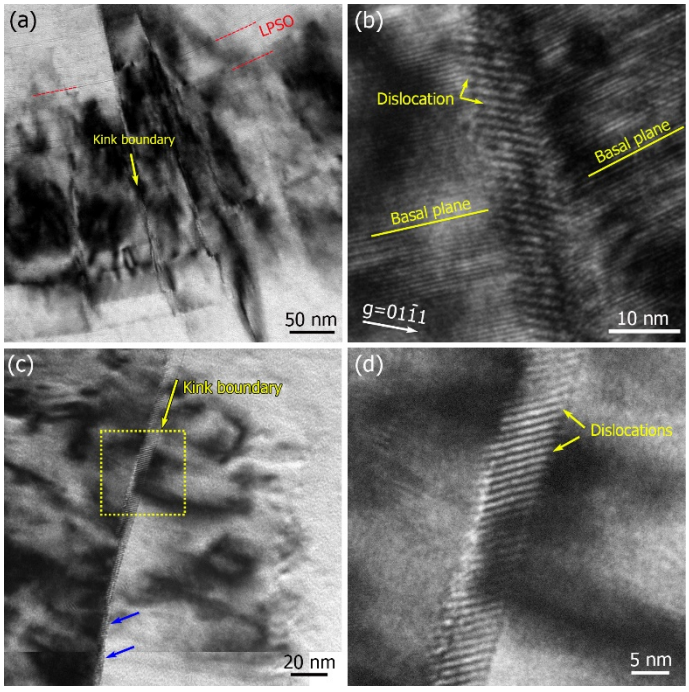

Figure 10 (a) TEM bright field image showing kink boundaries arranged in a rotational morphology inside LPSO/Mg; (b) bright field image of a kink boundary in a LPSO/Mg region; the g vector indicated is to the left hand side of the kink boundary only; (c) bright field image of a kink boundary in the LPSO/Mg region; (d) the magnified image showing the dislocation wall.

Rotational kink boundaries were also observed in the upper right corner of the Figure 11a (kink boundaries were labelled), where the corresponding schematic drawing (in Figure 11d) shows the LPSO lamella (upper right corner, yellow lines) exhibits a round curvature due to the presence of the rotational kink boundaries (red dashed lines). Interestingly, the region shown by blue square in Figure 11a indicates the LPSO lamella also exhibit a round curvature but no kink boundaries was observed. A magnified image is shown in Figure 11b. The dark region is close to the Bragg condition for the (0001) reflection and it appears to be bounded by LPSO lamellae. This indicates that sudden orientation changes can be found in the LPSO/Mg interface. The red arrows point at

two misaligned LPSO lamellae, which most likely originates from the same LPSO lamella before deformation. This indicates that movement of the LPSO lamella has occurred in the c direction relative to the original LPSO lamella. After tilting a few degrees for better imaging, dislocations with <c> component (indicated by the yellow arrows, visible when g=0002) were observed in this area. This indicates the rotational morphology of the LPSO lamellar are formed by <c> component dislocations. As shown in left part of Figure 11d, the <c> component dislocations (green lines) can accommodate similar strains to that of kink boundaries and the LPSO lamellae bounding the <c> component dislocations exhibit a round curvature.

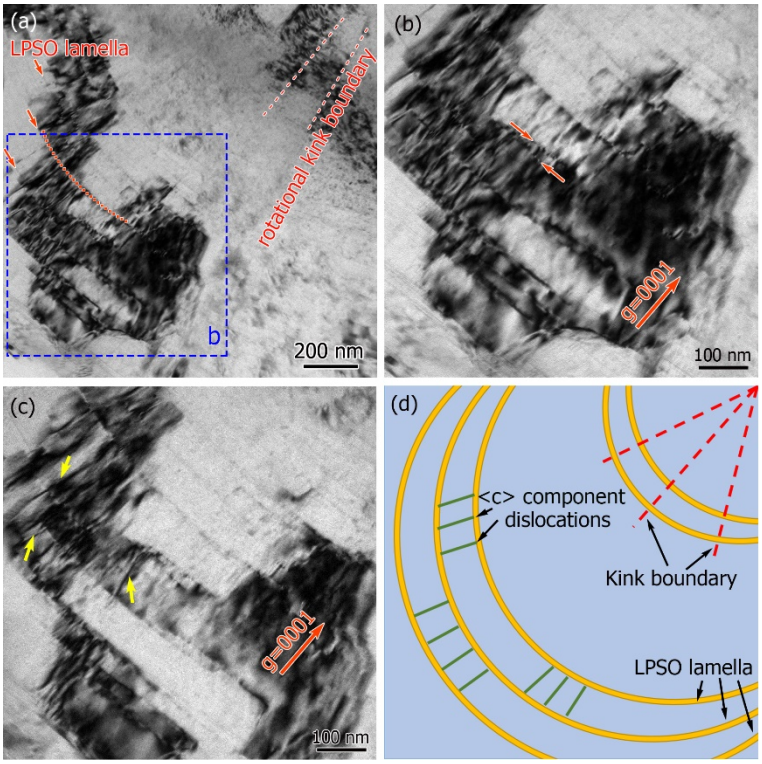

Figure 11 (a) Bright field image of a LPSO/Mg region showing rotational morphology; (b) a magnified image of the bottom left corner of Figure 11a; (c) same area as displayed in Figure 11b after tilting a few degrees. The yellow arrows indicate the dislocations with <c> component. (d) Schematic drawing corresponds to Figure 11a. The yellow lines represent LPSO lamella with a round curvature. The rotational kink boundaries are represented by red dashed line in the upper right corner. The green line represents the <c> component dislocations in the left part. Both kink

boundary and <c> component dislocation can form a rotational morphology of the LPSO lamella.

The morphology of the kink boundaries in the LPSO/Mg structure is similar to that in the LPSO phase. TKD results indicate that the rotation axis of the kink band is mainly distributed over a wide annulus including $\langle 1\bar{2}10\rangle$ and $\langle 0\bar{1}10\rangle$ zone axes. This is in general agreement with the rotation axes in the LPSO phase proposed by Hagihara et al [8], but less confined. Hagihara et al [8] suggested the rotation axis in LPSO is $\langle uvw0\rangle$ with a deviation angle less than 5^{o}. However, in the LPSO/Mg stucture, the deviation angle in the current study is much larger (around 20^{o}). In addition, the [0001] rotation axis in LPSO/Mg is also observed, which could have been caused by prismatic <a> slip [9], starting in the Mg matrix. The CRSS of prismatic <a> slip in the 18R LPSO phase is about 360 MPa [6], which is much higher than that of pure Mg (30-50 MPa [27]) or Mg-1.1 at% Y (about 70 MPa [28]).

The double kinking morphology in Figure 9 indicated two paired kink boundaries with opposite rotation directions in the LPSO/Mg structure. It is reasonable to believe that the paired kink boundaries were formed by dislocation pairs with opposite Burgers vectors, as proposed by Hess and Barrett [13]. It is likely that the outside paired kink boundaries formed first during deformation, then further stress led to the formation of paired kink bands within the original kind band.

Dislocations with <c> components were also frequently observed in the Mg structure (for example Figure 11c). Kim et al. [12] reported that <c+a> type dislocations are observed in the Mg matrix when thin LPSO lamellae are present. The non-basal dislocations provide an alternative deformation mode in comparison to the LPSO phase. As indicated in Figure 11, the adjacent area

outside a rotational kinked LPSO/Mg structure possesses non-basal dislocations. These can accommodate for similar strains along the <c> direction during deformation.

3.3 Dynamic recrystallisation (DRX) of Mg along the kink boundary

Figure 12a shows the forward scattered electron image of an LPSO/Mg structure with DRXed grains. The brighter LPSO lamellae are in the Mg matrix. Zig-sag shaped kinks can also be observed. Lots of $Mg_{24}Y_5$ particles are displayed in the lower right part of the image. The corresponding TKD orientation map (Figure 12b) indicates the orientation difference in the LPSO/Mg structure caused by the kink boundaries. The kink boundary areas exhibit different morphologies. Kink boundary c with the misorientation angle of about 26° is relatively straight, as shown in the TEM image in Figure 12c. Kink boundary d, on the other hand, has a misorientation angle of about 50°. Lots of grains with low misorientation angle grain boundaries are located along the curly kink boundary. Figure 12d shows that the small grains exhibit capsule-like shapes, where they have become elongated along the kink boundary d. These grains contain the original LPSO lamellae, which suggests that the boundaries have moved. Some small $Mg_{24}Y_5$ particles can be observed along the low angle grain boundaries as indicated by the arrow. In the area e (Figure 12 b), some recrystallised grains are observed, presumably from an original kink boundary. The misorientation angle measured from the left and right surrounding areas is about 110°, which is larger than kink boundaries c and d. The DRXed grains shown in Figure 12e have a polygon shape and they have grown into the deformed area.

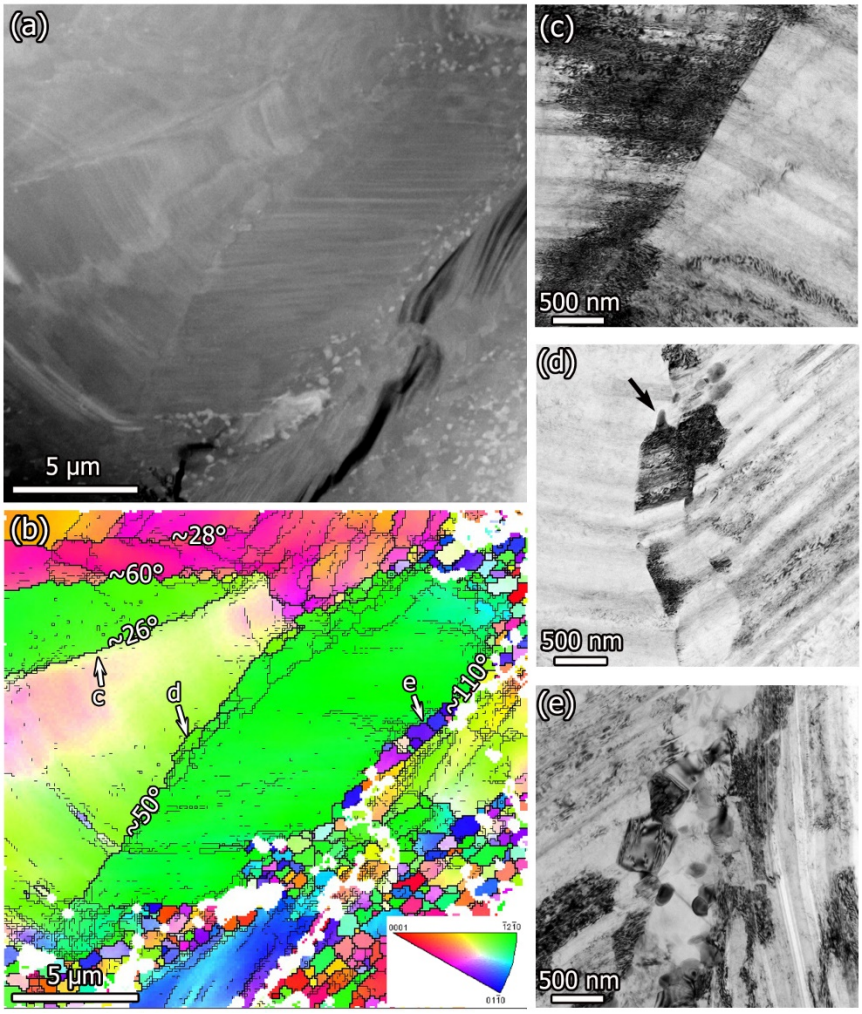

Figure 12 (a) Forward scattered image of a 3-pass ECAPed sample; (b) orientation map of Mg; the values inserted in the grain boundaries represent the misorientation angles; (c-e) TEM bright field images corresponding to the area in Figure 12b (the image has been rotated anticlockwise about 30-40° in the TEM).

When the misorientation angle of the kink boundary in the LPSO/Mg structure increases, grains with low angle grain boundaries have often been observed. This suggests that DRX occurred at the original kink boundaries, particularly at those with high misorientation angles. There are a few possible reasons that may account for the observation of DRX in Mg at kink boundaries.

Firstly, the nucleation of new grains is driven by the stored dislocations built up during the deformation. A kink boundary is composed of a higher density of dislocations and therefore a large strain energy. Secondly, kink boundaries can be an efficient barrier to dislocation movement during deformation. In the highly anisotropic LPSO/Mg structure, the mobile dislocations tend to be <a> dislocations on the basal plane, so a kink boundary makes it geometrically unfavourable for other mobile dislocations to pass. Thus, the DRXed grains tend to nucleate in the kink boundaries at high angles of misorientation.

5. Conclusions

An as-cast $Mg_{94}Zn_2Y_4$ alloy containing LPSO and $Mg_{24}Y_5$ as secondary phases was compressed and ECAP processed. The deformed microstructure was investigated, focusing in particular on the dislocation configurations in the kink boundaries of the LPSO phase and the LPSO/Mg structure. The following conclusions have been stated:

1. Kink bands were observed after 2% compression when the Mg alloy was deformed at room temperature. The low angle kink boundaries in the LPSO phase are essentially dislocation walls of <a> type basal dislocations (Burgers vector of $\frac{a}{3}\langle\bar{2}110\rangle$). When two sets of dislocations were observed, the rotation axis was found to be different from $\langle 1\bar{1}00\rangle$. The misorientation angles calculated using dislocation spacings, when based on the simple tilt low angle grain boundary model, are consistent with those measured off the TEM diffraction patterns.

2. TKD results show that the kink boundaries in the LPSO/Mg region have rotation axes mainly distributed in an annular area between $\langle 1\bar{2}10\rangle$ and $\langle 0\bar{1}10\rangle$.

3. Paired kink boundaries, which rotate in two opposite directions with a resulting total kink angle of about zero, have been observed in the LPSO/Mg structure. Double kinking, i.e. one pair of kink boundaries located inside another pair of kink boundaries, has also been observed.

4. The dislocation morphology of the kink boundaries in the LPSO/Mg structure is similar to that observed in the LPSO phase.

5. The kink boundaries in the LPSO/Mg structure are potential DRX nucleation sites for Mg grains during the ECAP. The DRXed Mg grains tend to form along kink boundaries that exhibit high angles of misorientation.

Acknowledgement

The authors thanks to Mr Dave Price for his help with the compression tests.

Data availability

The raw/processed data required to reproduce these findings cannot be shared at this time due to technical or time limitations.

References

[1] Y. Kawamura, K. Hayashi, A. Inoue, T. Masumoto. *Rapidly solidified powder metallurgy $Mg_{97}Zn_1Y_2$ alloys with excellent tensile yield strength above 600 MPa.* Materials Transactions 2001;**42**:1172-1176.

[2] A. Inoue, K. Kishida, H. Inui, K. Hagihara. *Compression of micro-pillars of a long period stacking ordered phase in the Mg-Zn-Y system.* MRS Online Proceedings Library 2013;**1516**:151-156.

[3] K. Hagihara, N. Yokotani, Y. Umakoshi. *Plastic deformation behavior of $Mg_{12}YZn$ with 18R long-period stacking ordered structure.* Intermetallics 2010;**18**(2):267-276.

[4] K. Hagihara, Y. Fukusumi, M. Yamasaki, T. Nakano, Y. Kawamura. *Non-basal slip systems operative in $Mg_{12}ZnY$ long-period stacking ordered (LPSO) Phase with 18R and 14H Structures.* Materials Transactions 2013;**54**(5):693-697.

[5] R. Chen, S. Sandlöbes, X. Zeng, D. Li, S. Korte-Kerzel, D. Raabe. *Room temperature deformation of LPSO structures by non-basal slip.* Materials Science and Engineering: A 2017;**682**(Supplement C):354-358.

[6] Y. Mine, R. Maezono, T. Mayama, J. Wu, Y.L. Chiu, P. Bowen, K. Takashima. *Plasticity and crack extension in single-crystalline long-period stacking ordered structures of $Mg_{85}Zn_6Y_9$ alloy under micro-bending.* Journal of Alloys and Compounds 2017;**718**:433-442.

[7] K. Hagihara, T. Okamoto, M. Yamasaki, Y. Kawamura, T. Nakano. *Electron backscatter diffraction pattern analysis of the deformation band formed in the Mg-based long-period stacking ordered phase.* Scripta Materialia 2016;**117**:32-36.

[8] K. Hagihara, M. Yamasaki, M. Honnami, H. Izuno, M. Tane, T. Nakano, Y. Kawamura. *Crystallographic nature of deformation bands shown in Zn and Mg-based long-period stacking ordered (LPSO) phase.* Philosophical Magazine 2014;**95**(2):132-157.

[9] M. Yamasaki, K. Hagihara, S.-i. Inoue, J.P. Hadorn, Y. Kawamura. *Crystallographic classification of kink bands in an extruded Mg–Zn–Y alloy using intragranular misorientation axis analysis.* Acta Materialia 2013;**61**(6):2065-2076.

[10] R. Chen, S. Sandlöbes, C. Zehnder, X. Zeng, S. Korte-Kerzel, D. Raabe. *Deformation mechanisms, activated slip systems and critical resolved shear stresses in an Mg-LPSO alloy studied by micro-pillar compression.* Materials and Design 2018;**154**:203-216.

[11] T. Matsumoto, M. Yamasaki, K. Hagihara, Y. Kawamura. *Configuration of dislocations in low-angle kink boundaries formed in a single crystalline long-period stacking ordered Mg-Zn-Y alloy.* Acta Materialia 2018;**151**:112-124.

[12] J.-K. Kim, S. Sandlöbes, D. Raabe. *On the room temperature deformation mechanisms of a Mg–Y–Zn alloy with long-period-stacking-ordered structures.* Acta Materialia 2015;**82**:414-423.

[13] J. Hess, C. Barrett. *Structure and nature of kink bands in zinc.* Transactions of the American Institute of Mining and Metallurgical Engineers 1949;**185**(9):599-606.

[14] F.C. Frank, A.N. Stroh. *On the theory of kinking.* Proceedings of the Physical Society. Section B 1952;**65**(10):811.

[15] X. Zhou, C. Liu, Y. Gao, S. Jiang, W. Liu, L. Lu. *Microstructure and mechanical properties of extruded Mg-Gd-Y-Zn-Zr alloys filled with intragranular LPSO phases.* Materials Characterization 2018;**135**:76-83.

[16] C. Xu, T. Nakata, X. Qiao, M. Zheng, K. Wu, S. Kamado. *Effect of LPSO and SFs on microstructure evolution and mechanical properties of Mg-Gd-Y-Zn-Zr alloy.* Scientific Reports 2017;**7**:40846.

[17] W. Liu, J. Zhang, C. Xu, X. Zong, W. Zhu, Q. Ma. *Precipitation behaviors of 14H LPSO lamellae in $Mg_{96}Gd_3Zn_{0.5}Ni_{0.5}$ alloys during severe plastic deformation.* Journal of Materials Science 2017;**52**(22):13271-13283.

[18] X.H. Shao, Z.Q. Yang, X.L. Ma. *Strengthening and toughening mechanisms in Mg-Zn-Y alloy with a long period stacking ordered structure.* Acta Materialia 2010;**58**(14):4760-4771.

[19] J. Yu, Z. Zhang, Q. Wang, X. Yin, J. Cui, H. Qi. *Dynamic recrystallization behavior of magnesium alloys with LPSO during hot deformation.* Journal of Alloys and Compounds 2017;**704**:382-389.

[20] W. Liu, Y. Ma, Y. Zhang, X. Fan, C. Xu, J. Zhang. *Two dynamic recrystallization processes in a high-performance extruded $Mg_{94.5}Y_2Gd_1Zn_2Mn_{0.5}$ alloy.* Materials Science and Engineering: A 2017;**690**:132-136.

[21] H. Liu, J. Ju, X. Yang, J. Yan, D. Song, J. Jiang, A. Ma. *A two-step dynamic recrystallization induced by LPSO phases and its impact on mechanical property of severe plastic deformation processed $Mg_{97}Y_2Zn_1$ alloy.* Journal of Alloys and Compounds 2017;**704**:509-517.

[22] Y. Chen, L. Jin, J. Dong, F. Wang, Y. Li, Y. Li, H. Pan, X. Nie. *Effects of LPSO/α-Mg interfaces on dynamic recrystallization behavior of $Mg_{96.5}Gd_{2.5}Zn_1$ alloy.* Materials Characterization 2017;**134**:253-259.

[23] X.-J. Zhou, C.-M. Liu, Y.-H. Gao, S.-N. Jiang, X.-Z. Han, Z.-Y. Chen. *Evolution of LPSO phases and their effect on dynamic recrystallization in a Mg-Gd-Y-Zn-Zr alloy.* Metallurgical and Materials Transactions A 2017;**48**(6):3060-3072.

[24] W. Liu, J. Zhang, L. Wei, C. Xu, X. Zong, J. Hao. *Extensive dynamic recrystallized grains at kink boundary of 14H LPSO phase in extruded $Mg_{92}Gd_3Zn_1Li_4$ alloy.* Materials Science and Engineering: A 2017;**681**:97-102.

[25] W.T. Read, *Dislocation in Crystals*1953: McGraw-Hill.

[26] D. Egusa, M. Yamasaki, Y. Kawamura, E. Abe. *Micro-kinking of the long-period stacking/order (LPSO) phase in a hot-extruded $Mg_{97}Zn_1Y_2$ Alloy.* Materials Transactions 2013;**54**(5):698-702.

[27] J.D. Robson, N. Stanford, M.R. Barnett. *Effect of precipitate shape and habit on mechanical asymmetry in magnesium alloys.* Metallurgical and Materials Transactions A 2013;**44**(7):2984-2995.

[28] T.M. H. Rikihisa, M. Tsushida, H. Kitahara, S. Ando. *Influence of Yttrium addition on plastic deformation of magnesium.* Materials Transactions 2017;**58**(12):1656-1663.